

Magneto-Optic Faraday Effect in Ultracold Atomic Gases

Zhen Zheng and Z. D. Wang*

Department of Physics and HKU-UCAS Joint Institute for Theoretical and Computational Physics at Hong Kong, The University of Hong Kong, Pokfulam Road, Hong Kong, China

We propose an arresting scheme for simulating the famous Faraday effect in ultracold atomic gases. Inspired by the similarities between the light field and the bosonic atoms, we represent the light propagation in medium by the atomic transport in accompany of the laser-atom interaction. The artificial magneto-optic Faraday effect is readily signaled by the spin imbalance of atoms, with the setup of laser fields offering a high controllability for quantum manipulation. Our proposal can be realized with current experimental techniques of ultracold atoms, and is quite promising for exploring and investigating the magneto-optic Faraday effect and associated physics.

Emulation of condensed-matter systems using ultracold atoms is an active area in the studies of quantum simulations [1–3]. This is because ultracold atoms can provide a versatile platform with a series of advantages: (i) The nontrivial interplay or external fields can be designed by the setup of the laser-atom interaction that can bring novel physics [4, 5]. (ii) The high controllability of the synthetic interplay and fields has promising applications such as exploring intriguing phase transitions [6–8] and critical phenomena [9, 10]. (iii) The absence of the disorder effect or impurities makes the well-isolated system ideally clean [11], and thereby facilitates the investigation for unraveling complex phenomena. Based on these features, a variety of quantum simulations using ultracold atoms have been successfully proposed in a broad range of interesting topics, for instance the ferromagnetism [12], quantum Hall effect [13, 14], atomtronic circuit [15, 16] and its hysteresis [17], atom transistor [18], and optical solenoid associated with magnetic flux [19].

In condensed-matter physics, it has been known that the transverse conductivity can play a key role in the magneto-optic effect [20]. It can be introduced by the interplay of the band exchange splitting and spin-orbit coupling in the magnetic medium [21]. When the light transmits from vacuum to the medium, the presence of the transverse conductivity hybrids the two polarized components of the photons and imposes a coherent phase to them during the light propagation. As the result, the polarized angle of the reflected and forward scattered light fields deviates from the one of the incident light, respectively known as the magneto-optic Kerr effect (MOKE) and Faraday effect (MOFE). Specifically, the magneto-optic effect can arise by virtue of the topological Hall effect, in which the rotated polarized angle is related to the topological invariant, known as the topological magneto-optic effect [22–24]. However, due to the photon absorption by the magnetic medium, MOFE is expected be detected in ultra-thin films. Since the rotation of the polarized angle is acquired during the light propagation, it dramatically drops in thinner films, and thereby the salient signal of MOFE is usually challenging

in ordinary magnetic mediums.

In this Letter, we propose a scheme for simulating MOFE in ultracold atoms. The following features of the atomic transport process [25] inspire us to draw an analogy to MOFE in terms of the bosonic cloud: (i) The hydrodynamics of the atomic cloud density can be semi-classically refined by the equation $\partial_t n + \mathbf{v} \cdot \nabla n = 0$ [26] and its linear dispersion shares the similarity of the light propagation. (ii) The internal levels of atoms provide extra degrees of freedom that are applied as pseudospins in cold-atom studies. In Bose gases, specifically the Bose-Einstein condensate (BEC), the wave function of different pseudospins are orthogonal, exhibiting the same property of the polarized components of the light. (iii) The artificial transverse conductivity can be generated by laser fields that couples different pseudospins, thus the laser-atom interacting region will play the role of the “medium”. The main results of this Letter show the simulated light field (i.e. the atomic density) displays distinguished signals before and after transmitting the simulated medium. It facilitates the observation to the artificial MOFE, and the high controllability unambiguously paves the way for manipulating MOFE and exploring its associated physics.

Model. — We consider the bosons with two hyperfine states that are denoted as spins \uparrow and \downarrow and used for mimicking the light polarization. In ultracold Bose gases, the atomic cloud can be loaded into two reservoirs separated by a mesoscopic channel [27–29]. By preparing the two reservoirs with a number imbalance, the atomic current can be observed through the channel, exhibiting the light propagation. The experimental setup is illustrated in FIG.1(a). We suppose the atomic cloud is prepared in the BEC phase. In the channel between the reservoirs, the atomic cloud can be approximately regarded as being confined in the harmonic trap potential $V_{\text{trap}}(\mathbf{r}) = \frac{1}{2}m\omega_{\text{trap}}(x^2 + y^2)$. In the section normal to the z direction, the wave function of the ground state is given by $\psi(\mathbf{r}) = e^{-(x^2 + y^2)/(2l_0^2)}/(\pi l_0^2)$, where $l_0 = \sqrt{\hbar/(m\omega_{\text{trap}})}$ [30]. Along the z direction, the atomic cloud flows at a center-of-mass (COM) velocity v_{cm} .

By implementing counter-propagating lasers along the

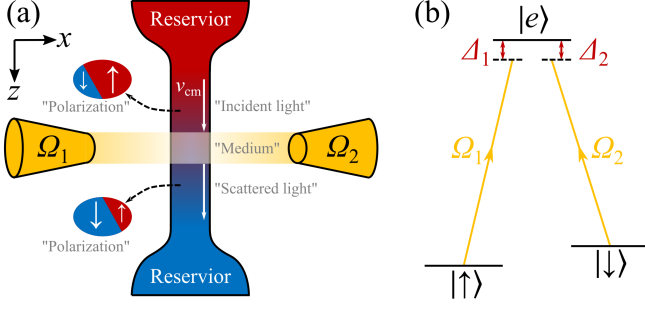


FIG. 1. (a) The experimental setup of the proposal: the light field is simulated via the atomic current between two reservoirs, in which the polarization of the light is characterized by the atomic spin imbalance. The laser-atom interacting region (yellow) plays the role of the medium in which the light can propagate. (b) Illustration of the atomic Λ -type transition: the two pseudospin states of atoms are coupled via a third excited states $|e\rangle$ by means of two Raman lasers $\Omega_{1,2}$ (yellow arrows). The detuning of each laser-atom interaction is denoted as $\Delta_{1,2}$.

x direction, a Raman transition between the two spins is driven via an auxiliary excited levels. It is a key to the artificial transverse conductivity. The transition is sketched in FIG.1(b). At low temperature, we assume the velocity fluctuation is much smaller than the laser field strength. In the COM reference frame, such a Λ system is governed by the following Hamiltonian,

$$H = [\hat{\Omega}_1(\mathbf{r})e^{-i\omega_1 t}|e\rangle\langle\uparrow| + \hat{\Omega}_2(\mathbf{r})e^{-i\omega_2 t}|e\rangle\langle\downarrow| + H.c.] + \sum_{\lambda=\uparrow,\downarrow,e} \Gamma_\lambda|\lambda\rangle\langle\lambda|. \quad (1)$$

Here $|\lambda\rangle$ with $\lambda = \uparrow, \downarrow, e$ denote the spin- \uparrow, \downarrow and excited states, respectively. $\Gamma_{\uparrow,\downarrow,e}$ are their corresponding level energies. $\hat{\Omega}_{\alpha=1,2}(\mathbf{r}) \equiv M_\alpha(\mathbf{r})e^{ik_\alpha x}$ where $M_\alpha(\mathbf{r})$ characterizes the laser field mode followed with the frequency ω_α as well as the standing-wave vector k_α . $H.c.$ stands for the Hermitian conjugation. We can assume the general form of the wave function for the three-level system as

$$|\psi\rangle = \sum_\lambda c_\lambda e^{-i\Gamma_\lambda t/\hbar} |\lambda\rangle. \quad (2)$$

According to the Schrödinger equation $i\partial_t|\psi\rangle = H|\psi\rangle$, the coefficient c_λ satisfies the following equations,

$$\begin{cases} i\hbar\partial_t c_\uparrow = \hat{\Omega}_1^*(\mathbf{r})e^{i\Delta_1 t/\hbar} c_e \\ i\hbar\partial_t c_\downarrow = \hat{\Omega}_2^*(\mathbf{r})e^{i\Delta_2 t/\hbar} c_e \\ i\hbar\partial_t c_e = \hat{\Omega}_1(\mathbf{r})e^{-i\Delta_1 t/\hbar} c_\uparrow + \hat{\Omega}_2(\mathbf{r})e^{-i\Delta_2 t/\hbar} c_\downarrow \end{cases}. \quad (3)$$

Here we have denoted the detuning as $\Delta_1 = \Gamma_e - \Gamma_\uparrow - \hbar\omega_1$ and $\Delta_2 = \Gamma_e - \Gamma_\downarrow - \hbar\omega_2$. For simplicity without loss of generality, we normalize the atomic densities by the total atomic number of the condensate. Thus the coefficient

c_λ obeys the constraint $\sum_\lambda |c_\lambda|^2 = 1$ due to the number conservation.

In order to give a simple physics picture for our proposal, we firstly consider the resonance condition $\Delta_1 = \Delta_2 = 0$. The atoms are initially prepared to reside in the two spin states that host the lowest energy. Due to spontaneous breaking the $U(1)$ symmetry, the BEC hosts distinguished phases for each spins [31]. Thereby, the initial state of the spinful system can be assumed as the form $|\psi_0\rangle = \cos\theta|\uparrow\rangle + \sin\theta e^{i\varphi}|\downarrow\rangle$. Here θ characterizes the number imbalance of spins, and φ describes the relative phase between the two spins. The solution to Eq.(3) is then given as follows,

$$\begin{cases} c_\uparrow = \cos\theta + F(\mathbf{r})\frac{\hat{\Omega}_1(\mathbf{r})}{\hat{\Omega}_R(\mathbf{r})}\{\cos[\hat{\Omega}_R(\mathbf{r})t/\hbar] - 1\} \\ c_\downarrow = \sin\theta e^{i\varphi} + F(\mathbf{r})\frac{\hat{\Omega}_2(\mathbf{r})}{\hat{\Omega}_R(\mathbf{r})}\{\cos[\hat{\Omega}_R(\mathbf{r})t/\hbar] - 1\} \\ c_e = -iF(\mathbf{r})\sin[\hat{\Omega}_R(\mathbf{r})t/\hbar] \end{cases}. \quad (4)$$

Here the dimensionless function is written as $F(\mathbf{r}) = [\hat{\Omega}_1(\mathbf{r})\cos\theta + \hat{\Omega}_2(\mathbf{r})e^{i\varphi}\sin\theta + H.c.]/[2\hat{\Omega}_R(\mathbf{r})]$. $\hat{\Omega}_R(\mathbf{r}) = \sqrt{|\hat{\Omega}_1(\mathbf{r})|^2 + |\hat{\Omega}_2(\mathbf{r})|^2}$ is the Rabi frequency.

For simplicity, we postulate the laser modes $M_{1,2}(\mathbf{r})$ to be slowly varied along the x direction in the atomic cloud. Since the laser fields are applied along the x direction, the atomic transition driven by them involves no momentum transfer in the z direction, and hence does not affect the atomic transport. In the laboratory frame, the Rabi frequency can be approximately expanded as $\hat{\Omega}_R(\mathbf{r}_{\text{cm}} + \mathbf{r}') \approx \hat{\Omega}_R(\mathbf{r}_{\text{cm}}) + \mathbf{r}' \cdot \nabla \hat{\Omega}_R(\mathbf{r}_{\text{cm}})$. Here the COM coordinate $\mathbf{r}_{\text{cm}} = v_{\text{cm}} t \hat{\mathbf{e}}_z$ with $\hat{\mathbf{e}}_{x,y,z}$ being the unit vector. Since the laser fields are spatially uniform along the trajectory direction, quantities that depend only on \mathbf{r}_{cm} can be regarded as constants hereafter. We denote the gradient of the laser field as $\nabla \hat{\Omega}_R(\mathbf{r}_{\text{cm}}) \equiv A \hat{\mathbf{e}}_x$. This can be attainable in practice, for instance by using Gaussian beams whose center deviates from the atomic COM trajectory.

In a steady transport case, the atomic current is incompressible along the trajectory direction. The density per unit of length along the z direction can be obtained by $n_\sigma = \int |c_\sigma \psi(\mathbf{r})|^2 dx dy$ for spin- $\sigma = \uparrow, \downarrow$ components. We suppose the spatial scale of the atomic cloud is tremendously larger than the laser wavelengths, i.e. $k_1 l_0, k_2 l_0 \gg 1$. Then the rapid spatial modulated terms such as $\cos(k_1 x)$ and $\cos(k_2 x + \varphi)$ in $F(\mathbf{r})$ will be averaged to exponentially vanish when integrating out the spatial coordinates [32]. After detailed derivations, the forms of densities are given as

$$\begin{cases} n_\uparrow = \cos^2\theta + \Omega_1^2 K_1(t) \cos^2\theta + \Omega_1^2 K_2(t) \\ n_\downarrow = \sin^2\theta + \Omega_2^2 K_1(t) \sin^2\theta + \Omega_2^2 K_2(t) \end{cases}, \quad (5)$$

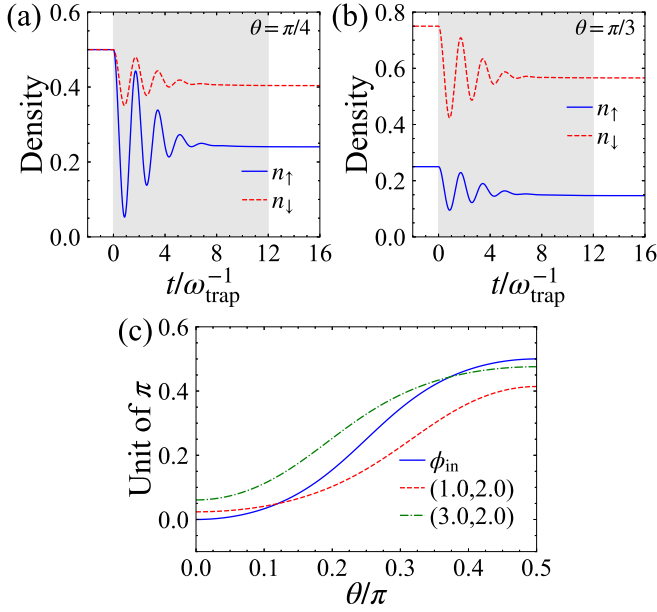


FIG. 2. (a)-(b) The evolutions of atomic densities at resonance condition. We set $\theta = \pi/4$ in (a) and $\pi/3$ in (b). Other parameters are $(\Omega_1, \Omega_2) = (3.0, 2.0)\hbar\omega_{\text{trap}}$, and $\tau_c^{-1} = 0.2\omega_{\text{trap}}$. The regions of the atomic cloud interacting with lasers are highlighted in gray. (c) The polarized angles of the simulated light as functions of θ : ϕ_{in} (blue-solid line), ϕ_{sc} at $(\Omega_1, \Omega_2) = (1.0, 2.0)\hbar\omega_{\text{trap}}$ (red-dashed line), and ϕ_{sc} at $(3.0, 2.0)$ (green-dash-dotted line).

where the time-dependent functions are expressed as

$$K_1(t) = [\cos(\Omega_R t/\hbar)e^{-t^2/\tau_c^2} - 1]/\Omega_R^2, \quad (6)$$

$$K_2(t) = \mathcal{F}[\cos(2\Omega_R t/\hbar)e^{-4t^2/\tau_c^2} - 4\cos(\Omega_R t/\hbar)e^{-t^2/\tau_c^2} + 3]/(2\Omega_R^2), \quad (7)$$

and $\mathcal{F} = (\Omega_1^2 \cos^2 \theta + \Omega_2^2 \sin^2 \theta)/(2\Omega_R^2)$. We have denoted $\Omega_{1,2} = M_{1,2}(\mathbf{r}_{\text{cm}})$ and $\Omega_R = \hat{\Omega}_R(\mathbf{r}_{\text{cm}})$. The decay time τ_c is defined as $\tau_c = 2\hbar/(A l_0)$.

From Eq.(5), one can see that in the presence of the laser field gradient A , the Rabi oscillations are exponentially suppressed. Similar phenomena can be evidenced by experiments yet in a two-level system [33]. The atomic cloud will evolve to a steady state in which the densities saturate to

$$\begin{cases} n_{\uparrow}(t \rightarrow \infty) = \cos^2 \theta - \frac{\Omega_1^2}{\Omega_R^2} \cos^2 \theta + \frac{3\mathcal{F}}{2} \frac{|\Omega_1|^2}{\Omega_R^2} \\ n_{\downarrow}(t \rightarrow \infty) = \sin^2 \theta - \frac{\Omega_2^2}{\Omega_R^2} \sin^2 \theta + \frac{3\mathcal{F}}{2} \frac{|\Omega_2|^2}{\Omega_R^2} \end{cases}. \quad (8)$$

The dynamic evolutions are shown in FIG.2(a) and (b) for different initial setups. For simplicity, we have assumed the atomic cloud in motion enters the laser region at $t = 0$, and leaves it after the cloud fully evolved to the steady state. It can be guaranteed by preparing the width of the laser region $L > v_{\text{cm}}\tau_c$.

As we use the bosonic atoms to represent the light field, the polarized angle ϕ of the simulated light field is defined by the atomic densities,

$$\phi = \tan^{-1}[n_{\downarrow}(t)/n_{\uparrow}(t)], \quad (9)$$

which is time dependent. In particular, the polarized angle of the incident light is expressed as $\phi_{\text{in}} = \tan^{-1}(\tan^2 \theta)$, while for the scattered light is calculated by $\phi_{\text{sc}} = \tan^{-1}[n_{\downarrow}(\infty)/n_{\uparrow}(\infty)]$ (c.f. Eq.(8)). In FIG.2(c), we can see the polarized angle is changed after the light passes through the simulated medium, exhibiting the manifest feature of MOFE. The signal of the artificial MOFE (i.e. the rotated polarized angle) not only depends on the parameter θ of initial setups, but is also controllable by the laser field strengths $\Omega_{1,2}$.

Detuned case.— The resonance condition used in the above discussions will introduce the additional heating effect that are frustrated to the practical experiments such as suppressing the lifetime of ultracold atoms [34]. However, we remark that the resonance condition in the Λ system is not necessary, instead the proposal still works when the laser-atom interaction is prepared with a detuning $\Delta_1 = \Delta_2 = \Delta \neq 0$. It has a crucial advantage that, at the fully far detuned regime (i.e. $\Delta \gg |\hat{\Omega}_{1,2}(\mathbf{r})|$), the heating effect can prominently suppressed and thereby facilitates the realization of the proposal. At this time, the solution of Eq.(3) takes the following form [32]

$$\begin{cases} c_1 = \cos \theta + F(\mathbf{r})\hat{\Omega}_1^*(\mathbf{r}) \sum_{\alpha=\pm} \alpha \frac{e^{i\hat{\Omega}_R^\alpha(\mathbf{r})t/\hbar} - 1}{\hat{\Omega}_R^\alpha(\mathbf{r})} \\ c_2 = \sin \theta e^{i\varphi} + F(\mathbf{r})\hat{\Omega}_2^*(\mathbf{r}) \sum_{\alpha=\pm} \alpha \frac{e^{i\hat{\Omega}_R^\alpha(\mathbf{r})t/\hbar} - 1}{\hat{\Omega}_R^\alpha(\mathbf{r})} \\ c_e = -F(\mathbf{r})e^{-i\Delta t/\hbar} \sum_{\alpha=\pm} \alpha e^{i\hat{\Omega}_R^\alpha(\mathbf{r})t/\hbar} \end{cases} \quad (10)$$

where the dimensionless function is rewritten as $F(\mathbf{r}) = [\hat{\Omega}_1(\mathbf{r}) \cos \theta + \hat{\Omega}_2(\mathbf{r})e^{i\varphi} \sin \theta + H.c.]/\{2[\hat{\Omega}_R^+(\mathbf{r}) - \hat{\Omega}_R^-(\mathbf{r})]\}$. We can see that the Rabi oscillations are split into two branches whose frequencies are expressed as $\hat{\Omega}_R^\pm(\mathbf{r}) = \Delta/2 \pm \sqrt{|\hat{\Omega}_1(\mathbf{r})|^2 + |\hat{\Omega}_2(\mathbf{r})|^2 + \Delta^2/4}$.

The evolutions of the atomic densities share the same form of Eq.(5), but the time-dependent functions are instead rewritten as

$$\begin{aligned} K_1(t) &= \frac{1}{\Omega_R^+ + \Omega_R^-} \sum_{\alpha=\pm} \frac{\cos(\Omega_R^\alpha t/\hbar)e^{-t^2/\tau_{c\alpha}^2} - 1}{\Omega_R^\alpha}, \quad (11) \\ K_2(t) &= \sum_{\alpha=\pm} \frac{2\mathcal{F}}{|\Omega_R^\alpha|^2} + \frac{2\mathcal{F}}{\Omega_R^+ \Omega_R^-} \cos[(\Omega_R^+ + \Omega_R^-)t/\hbar]e^{-4t^2/\tau_c^2} \\ &\quad - \sum_{\alpha,\alpha'} \frac{2\mathcal{F}}{\Omega_R^\alpha \Omega_R^{\alpha'}} \cos(\Omega_R^\alpha t/\hbar)e^{-t^2/\tau_{c\alpha}^2} + \frac{2\mathcal{F}}{\Omega_R^+ \Omega_R^-} \quad (12) \end{aligned}$$

with $\mathcal{F} = (\Omega_1^2 \cos^2 \theta + \Omega_2^2 \sin^2 \theta)/[2(\Omega_R^+ + \Omega_R^-)^2]$. We have denoted $\Omega_R^\pm = \pm \hat{\Omega}_R^\pm(\mathbf{r}_{\text{cm}})$, $A_\pm = \pm \nabla_x \hat{\Omega}_R^\pm(\mathbf{r}_{\text{cm}})$,

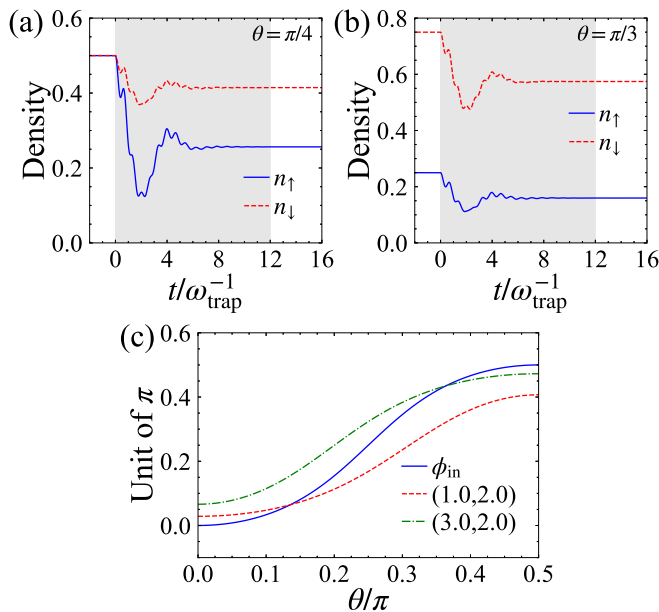


FIG. 3. (a)-(b) The evolutions of atomic densities with a detuning $\Delta = 8.0\hbar\omega_{\text{trap}}$. We set $\theta = \pi/4$ in (a) and $\pi/3$ in (b). Other parameters are $(\Omega_1, \Omega_2) = (3.0, 2.0)\hbar\omega_{\text{trap}}$, and $\tau_{c\pm}^{-1} = 0.2\omega_{\text{trap}}$. The regions of the atomic cloud interacting with lasers are highlighted in gray. (c) The polarized angles of the simulated light as functions of θ : ϕ_{in} (blue-solid line), ϕ_{sc} at $(\Omega_1, \Omega_2) = (1.0, 2.0)\hbar\omega_{\text{trap}}$ (red-dashed line), and ϕ_{sc} at $(3.0, 2.0)$ (green-dash-dotted line).

$\tau_{c\pm} = 2\hbar/(A_{\pm}l_0)$, and $\tilde{\tau}_{c\pm}^{-1} = \tau_{c+}^{-1} + \tau_{c-}^{-1}$. It is easy to demonstrated that $K_{1,2}(t)$ reduces to the form given in Eqs.(6) and (7) at resonance $\Delta = 0$. The evolutions are plotted in FIG.3(a) and (b). Likewise as in a similar way to the resonance condition, the polarized angle of the incident light is shifted after passing through the medium, as shown in FIG.3(c).

We comment that the decay time τ_{c+} and τ_{c-} are indeed identical. This is because the spatial dependence of $\hat{\Omega}_R^{\pm}(\mathbf{r})$ originates from the laser field modes $M_{1,2}(\mathbf{r})$, and hence their gradients A_{\pm} are equal to each other. In comparison between FIG.2(c) and FIG.3(c), we find that the rotated polarized angles is insensitive to the detuning Δ . This is because in the steady state, Δ only affects the Rabi frequencies $\hat{\Omega}_R^{\pm}(\mathbf{r})$, which is nearly canceled out in the calculation using Eq.(9).

Discussions. — In general, the Bose gas is composed of not only the BEC component but also the non-condensed one. This is usually evidenced by the contrast of condensate densities in spatial and momentum spaces [35–37]. In the plane normal to the trajectory direction, the spatial profile of the non-condensed wave function can be given by $\psi_{\text{nc}}(\mathbf{r}) = e^{-(x^2+y^2)/(2l_{\text{nc}}^2)}/(\pi l_{\text{nc}}^2)$ with $l_{\text{nc}} = \sqrt{k_B T/(m\omega_{\text{trap}}^2)}$ at temperature T . Similar to the results of the BEC case, the laser field gradients can also lead to the exponential damping in the evolution of

atomic densities. However, the decay times are approximately estimated as $\tau_{c\pm}^{\text{nc}} = \tau_{c\pm}l_0/l_{\text{nc}}$ instead. It implies that the densities of the non-condensed component will evolve to the steady state faster at higher temperature.

The presence of the non-condensed component does not alter the results or arguments obtained before. This can be explained as follows. Outside the laser-atom interacting region, there is no coupling between the two spins. The system of each spin reduces to the ideal Bose gas confined in a two-dimensional harmonic trap potential. It can be demonstrated that [32], in a bosonic system composed of N_{total} atoms, the atomic number of the non-condensed component N_{nc} is determined by $N_{\text{nc}}/N_{\text{total}} = (T/T_c)^{5/2}$ below T_c . Here T_c stands for the critical temperature for the phase transition that BEC vanishes. We can find that N_{nc} depends only on the temperature T , and is proportional to the BEC number: $N_0 = N_{\text{total}} - N_{\text{nc}} = [(T_c/T)^{5/2} - 1]N_{\text{nc}}$. Therefore, the density ratio between opposite spins in the non-condensed component is identical to the results obtained in BEC. It reveals the polarized angles of the two components evolve in the same way, yet are damped in different decay time.

The excited state $|e\rangle$ is occupied even after the atoms evolve to the steady state. As the atomic density of each spin respectively characterizes the amplitudes of the polarized light field, the residence number n_e can be used to represent the absorbance ratio of the the simulated medium. However, the ubiquitous spontaneous emission of the atoms will lead the decay from the excited state $|e\rangle$ to the two spin states that host the lower energy. In the Λ system of the proposal, there are two dressed states that are mutually orthogonal: the bright one $|\psi_B\rangle = \Omega_1/\Omega_R|\uparrow\rangle + \Omega_2/\Omega_R|\downarrow\rangle$ which is coupled to $|e\rangle$ through the laser fields, and the dark one $|\psi_D\rangle = -\Omega_2/\Omega_R|\uparrow\rangle + \Omega_1/\Omega_R|\downarrow\rangle$ which is decoupled from $|e\rangle$ and $|\psi_B\rangle$. For the sake of the spontaneous emission, the atoms eventually evolve to the dark state $|\psi_D\rangle$. The dynamic evolution is known as the coherent population trapping [38] and is widely applied in the laser cooling [39, 40]. The spin imbalance of the dark state, i.e. the polarized angle of the scattered light, is solely determined by the laser field strength $\Omega_{1,2}$ and is independent from the polarized angle of the incident light. At this time, the laser-atom region plays the role of a polarizer. It filters the light with a specific polarized angle $\phi = \tan^{-1}(\Omega_1^2/\Omega_2^2)$. Therefore in order to evidence MOFE, the lifetime of the excited state $|e\rangle$ is required to exceed the decay time τ_c . A potential candidate for implementing the proposal is the alkaline-earth-metal(-like) atoms, which have metastable states with the long lifetime of about hundred milliseconds or exceeded. For example of ^{88}Sr , by setting $\omega_{\text{trap}} \approx 2\pi \times 200\text{Hz}$, the condensate lengths are evaluated as $l_0 \approx 0.75\mu\text{m}$ and $l_{\text{nc}} \approx 7.7\mu\text{m}$ at the μK level. If we choose the laser field gradient as $A \approx 20\text{kHz/mm}$, the decay time is obtained

as $\tau_c \approx 21\text{ms}$ and $\tau_c^{\text{nc}} \approx 2.0\text{ms}$. Noticing that the Rabi oscillations decay exponentially as e^{-t^2/τ_c^2} , the system will evolve to the steady state within several milliseconds. Therefore, the usage of alkaline-earth-metal atoms is feasible for evidencing the artificial MOFE.

In summary, we have proposed an experimentally feasible scheme for simulating MOFE in ultracold atoms. The artificial MOFE originates from the laser-atom interaction by representing the light propagation in terms of the atoms. It can be realized and observable based on existing experimental techniques. The proposal broadens the concept of MOFE to the ultracold atomic gases, and offers a reliable platform for investigating MOFE using ultracold atoms.

Acknowledgements.— We acknowledge S. Z. Zhang for helpful discussions. This work was supported by the Key-Area Research and Development Program of Guangdong Province (Grant No. 2019B030330001), the National Key Research and Development Program of China (Grant No. 2016YFA0301800), the GRF (No.: HKU173057/17P) and CRF (No.: C6005-17G) of Hong Kong.

* zwang@hku.hk

- [1] M. Lewenstein, A. Sanpera, V. Ahufinger, B. Damski, A. Sen(De), and U. Sen, *Adv. Phys.* **56**, 243 (2007).
- [2] I. M. Georgescu, S. Ashhab, and F. Nori, *Rev. Mod. Phys.* **86**, 153 (2014).
- [3] M. S. Safronova, D. Budker, D. DeMille, D. F. J. Kimball, A. Derevianko, and C. W. Clark, *Rev. Mod. Phys.* **90**, 025008 (2018).
- [4] J. Dalibard, F. Gerbier, G. Juzeliūnas, and P. Öhberg, *Rev. Mod. Phys.* **83**, 1523 (2011).
- [5] N. Goldman, G. Juzeliūnas, P. Öhberg, and I. B. Spielman, *Rep. Prog. Phys.* **77**, 126401 (2014).
- [6] M. Greiner, O. Mandel, T. Esslinger, T. W. Hänsch, and I. Bloch, *Nature* **415**, 39 (2002).
- [7] T. Stöferle, H. Moritz, C. Schori, M. Köhl, and T. Esslinger, *Phys. Rev. Lett.* **92**, 130403 (2004).
- [8] I. B. Spielman, W. D. Phillips, and J. V. Porto, *Phys. Rev. Lett.* **98**, 080404 (2007).
- [9] I. Bloch, *Nat. Phys.* **1**, 23 (2005).
- [10] J. O. Andersen, U. Al Khawaja, and H. T. C. Stoof, *Phys. Rev. Lett.* **88**, 070407 (2002).
- [11] I. Bloch, J. Dalibard, and S. Nascimbène, *Nat. Phys.* **8**, 267 (2012).
- [12] C. V. Parker, L.-C. Ha, and C. Chin, *Nat. Phys.* **9**, 769 (2013).
- [13] M. Aidelsburger, M. Atala, M. Lohse, J. T. Barreiro, B. Paredes, and I. Bloch, *Phys. Rev. Lett.* **111**, 185301 (2013).
- [14] H. Miyake, G. A. Siviloglou, C. J. Kennedy, W. C. Burton, and W. Ketterle, *Phys. Rev. Lett.* **111**, 185302 (2013).
- [15] R. A. Pepino, J. Cooper, D. Z. Anderson, and M. J. Holland, *Phys. Rev. Lett.* **103**, 140405 (2009).
- [16] F. Jendrzejewski, S. Eckel, N. Murray, C. Lanier, M. Edwards, C. J. Lobb, and G. K. Campbell, *Phys. Rev. Lett.* **113**, 045305 (2014).
- [17] S. Eckel, J. G. Lee, F. Jendrzejewski, N. Murray, C. W. Clark, C. J. Lobb, W. D. Phillips, M. Edwards, and G. K. Campbell, *Nature* **506**, 200 (2014).
- [18] Z. Zhang, V. Dunjko, and M. Olshanii, *New J. Phys.* **17**, 125008 (2015).
- [19] B. Wang, F. N. Ünal, and A. Eckardt, *Phys. Rev. Lett.* **120**, 243602 (2018).
- [20] P. S. Pershan, *J. Appl. Phys.* **38**, 1482 (2004).
- [21] H. Ebert, *Rep. Prog. Phys.* **59**, 1665 (1996).
- [22] W.-K. Tse and A. H. MacDonald, *Phys. Rev. Lett.* **105**, 057401 (2010).
- [23] W.-K. Tse and A. H. MacDonald, *Phys. Rev. B* **84**, 205327 (2011).
- [24] W. Feng, J.-P. Hanke, X. Zhou, G.-Y. Guo, S. Blügel, Y. Mokrousov, and Y. Yao, *Nat. Commun.* **11**, 118 (2020).
- [25] C.-C. Chien, S. Peotta, and M. Di Ventra, *Nat. Phys.* **11**, 998 (2015).
- [26] F. Dalfovo, S. Giorgini, L. P. Pitaevskii, and S. Stringari, *Rev. Mod. Phys.* **71**, 463 (1999).
- [27] J.-P. Brantut, J. Meineke, D. Stadler, S. Krinner, and T. Esslinger, *Science* **337**, 1069 (2012).
- [28] S. Krinner, D. Stadler, J. Meineke, J.-P. Brantut, and T. Esslinger, *Phys. Rev. Lett.* **110**, 100601 (2013).
- [29] S. Krinner, D. Stadler, D. Husmann, J.-P. Brantut, and T. Esslinger, *Nature* **517**, 64 (2014).
- [30] C. J. Pethick and H. Smith, *Bose-Einstein Condensation in Dilute Gases* (Cambridge University Press, 2008).
- [31] M. R. Andrews, C. G. Townsend, H.-J. Miesner, D. S. Durfee, D. M. Kurn, and W. Ketterle, *Science* **275**, 637 (1997).
- [32] See the Supplemental Materials.
- [33] A. Daniel, R. Agou, O. Amit, D. Groswasser, Y. Japha, and R. Folman, *Phys. Rev. A* **87**, 063402 (2013).
- [34] D. S.-K. W. Ketterle, D.S. Durfee, in *Bose-Einstein Condensation in Atomic Gases, Proceedings of the International School of Physics Enrico Fermi, Course CXL*, edited by C. E. W. M. Inguscio, S. Stringari (IOS Press, Amsterdam, 1999) pp. 67–176.
- [35] M. H. Anderson, J. R. Ensher, M. R. Matthews, C. E. Wieman, and E. A. Cornell, *Science* **269**, 198 (1995).
- [36] K. B. Davis, M.-O. Mewes, M. R. Andrews, N. J. van Druten, D. S. Durfee, D. M. Kurn, and W. Ketterle, *Phys. Rev. Lett.* **75**, 3969 (1995).
- [37] C. C. Bradley, C. A. Sackett, J. J. Tollett, and R. G. Hulet, *Phys. Rev. Lett.* **75**, 1687 (1995).
- [38] M. O. Scully and M. S. Zubairy, *Quantum Optics* (Cambridge University Press, 1997).
- [39] A. Aspect, E. Arimondo, R. Kaiser, N. Vansteenkiste, and C. Cohen-Tannoudji, *Phys. Rev. Lett.* **61**, 826 (1988).
- [40] A. Aspect, E. Arimondo, R. Kaiser, N. Vansteenkiste, and C. Cohen-Tannoudji, *J. Opt. Soc. Am. B* **6**, 2112 (1989).